An anion-immobilized composite electrolyte for dendrite-free lithium metal anodes

Chen-Zi Zhao[a,1], Xue-Qiang Zhang[a,1], Xin-Bing Cheng[a,1], Rui Zhang[a], Rui Xu[b], Peng-Yu Chen[a], Hong-Jie Peng[a], Jia-Qi Huang[b], and Qiang Zhang[a,2]

[a]Beijing Key Laboratory of Green Chemical Reaction Engineering and Technology, Department of Chemical Engineering, Tsinghua University, Beijing 100084, China; and [b]Advanced Research Institute for Multidisciplinary Science, Beijing Institute of Technology, Beijing 100081, China

Edited by Thomas E. Mallouk, The Pennsylvania State University, University Park, PA, and approved September 8, 2017 (received for review May 22, 2017)

Lithium metal is strongly regarded as a promising electrode material in next-generation rechargeable batteries due to its extremely high theoretical specific capacity and lowest reduction potential. However, the safety issue and short lifespan induced by uncontrolled dendrite growth have hindered the practical applications of lithium metal anodes. Hence, we propose a flexible anion-immobilized ceramic–polymer composite electrolyte to inhibit lithium dendrites and construct safe batteries. Anions in the composite electrolyte are tethered by a polymer matrix and ceramic fillers, inducing a uniform distribution of space charges and lithium ions that contributes to a dendrite-free lithium deposition. The dissociation of anions and lithium ions also helps to reduce the polymer crystallinity, rendering stable and fast transportation of lithium ions. Ceramic fillers in the electrolyte extend the electrochemically stable window to as wide as 5.5 V and provide a barrier to short circuiting for realizing safe batteries at elevated temperature. The anion-immobilized electrolyte can be applied in all–solid-state batteries and exhibits a small polarization of 15 mV. Cooperated with $LiFePO_4$ and $LiNi_{0.5}Co_{0.2}Mn_{0.3}O_2$ cathodes, the all–solid-state lithium metal batteries render excellent specific capacities of above 150 $mAh{\cdot}g^{-1}$ and well withstand mechanical bending. These results reveal a promising opportunity for safe and flexible next-generation lithium metal batteries.

lithium metal anode | composite electrolyte | all–solid-state lithium batteries | immobilized anion | lithium dendrite

The expanding demand for energy storage calls for safe, high-energy density, and low-cost batteries. Lithium (Li) metal with a very high theoretical specific capacity of 3,860 $mAh{\cdot}g^{-1}$ and the lowest reduction potential (−3.04 V vs. standard hydrogen electrode) has been strongly regarded as a promising anode material in next-generation rechargeable batteries (1–3). However, the uncontrolled dendrite growth during Li plating and stripping results in potential issues such as short circuiting and short lifespan (4), hindering the practical applications of Li metal batteries (LMBs) over decades (5).

Generally, Li metal anodes are operated in organic liquid electrolytes, which compromise on the viscosity and dielectric constant. Those organic electrolytes react with the Li metal, forming a solid-electrolyte interphase (SEI) (6–8). However, the as-formed SEI is heterogeneous, which induces the inhomogeneous Li deposition (9, 10). Consequently, Li dendrites are generated inevitably on a working anode in liquid electrolytes. Moreover, the natural SEI is too fragile to tolerate the volumetric and morphological change of Li metal anode (11). With the increasing cycle number, the repeated crack and formation of the SEI accelerate the continual consumption of both Li metal and electrolyte, increasing the interfacial resistance between the Li anode and electrolyte (12). It also causes a serious safety hazard when Li dendrites penetrate through a separator and contact with a cathode directly (13).

Extensive efforts have been devoted to solving the above problems, including electrolyte additives (7, 14), stable nanostructured Li metal hosts (15), and the separator modification (16, 17). Despite these efforts varying from each other, most of them aim to adjust the ion distribution during cycling. In terms of the ion distribution, space-charge theory is widely accepted in cases of nonaqueous electrolytes. In this theory, the electrolyte is divided into a quasi-neutral region and a space-charge region. The quasi-neutral region approaches the cathode side, at which the ion transfer is governed by diffusion. In contrast, when ions travel close to the anode side, the ion transport is mainly driven by the electric field, leaving a space-charge region that accounts for ramified Li metal growth. Consequently, it is rewarding to design the electrolyte, which can regulate the ion distribution (including both Li cations and the counter anions) to inhibit Li dendrite growths (18, 19). Recently, several lithiophilic matrices were proposed to regulate the diffusion behavior of Li ions, realizing uniform distribution of Li ions near the anode side (6, 20, 21). Archer and coworkers (22, 23) pioneered the concept of anion regulation and found that a portion of immobilized anions (even as small as 10%) in liquid electrolytes contribute to stable electrodeposition and 10-fold increased cell lifetime (24).

Immobilizing anions in liquid electrolytes improves the cycling performance of Li metal anodes significantly. However, such an approach is unreliable, owing to the intrinsic reactivity of Li metal and the fragile SEI formed in liquid electrolytes (25). Moreover, the liquid electrolyte also suffers from leakage, fire, and explosion, hindering the development of next-generation LMBs seriously. To address the aforementioned issues and build a safe battery, the solid electrolyte is regarded as one of the ultimate choices to operate Li metal anodes safely even at elevated temperature, which can avoid leaking, combusting, and corroding Li metal inherently (26–29). The excellent electrochemical stability of solid

Significance

The Li metal electrode is regarded as a "Holy Grail" anode for next-generation batteries due to its extremely high theoretical capacity and lowest reduction potential. Unfortunately, uncontrolled dendrite growth leads to serious safety issues. This work realizes a dendrite-free Li metal anode by introducing an anion-immobilized composite solid electrolyte, where anions are tethered to polymer chains and ceramic particles. Immobilized anions contribute to uniform distribution of Li ions and dendrite-free Li deposition. The flexible electrolyte can be applied in all–solid-state Li metal batteries with excellent specific capacities. This work demonstrates a concept to adjust ion distribution based on solid-state electrolytes for safe dendrite-free Li anodes, paving the way to practical Li metal batteries.

Author contributions: C.-Z.Z., X.-Q.Z., and Q.Z. designed research; C.-Z.Z., X.-Q.Z., X.-B.C., R.Z., R.X., P.-Y.C., H.-J.P., and J.-Q.H. performed research; R.Z., R.X., P.-Y.C., H.-J.P., and J.-Q.H. contributed new reagents/analytic tools; C.-Z.Z., X.-Q.Z., X.-B.C., R.Z., R.X., P.-Y.C., H.-J.P., J.-Q.H., and Q.Z. analyzed data; and C.-Z.Z., X.-Q.Z., X.-B.C., R.Z., J.-Q.H., and Q.Z. wrote the paper.

The authors declare no conflict of interest.

This article is a PNAS Direct Submission.

[1]C.-Z.Z., X.-Q.Z., and X.-B.C. contributed equally to this work.

[2]To whom correspondence should be addressed. Email: zhang-qiang@mails.tsinghua.edu.cn.

This article contains supporting information online at www.pnas.org/lookup/suppl/doi:10.1073/pnas.1708489114/-/DCSupplemental.

electrolytes enables high-voltage cathode materials to pair with a Li metal anode, widening the working voltage window and therefore increasing the gravimetric energy density (30, 31). Besides, solid-state batteries can be packed more densely in a flexible configuration, increasing the volumetric energy density as well (32, 33).

In this contribution, we develop an anion-immobilized solid-state composite electrolyte to protect Li metal anodes (Fig. 1). Garnet-type Al-doped $Li_{6.75}La_3Zr_{1.75}Ta_{0.25}O_{12}$ (LLZTO) ceramic particles are well dispersed in a polymer–Li salt matrix to synthesize a polyethylene oxide (PEO)–lithium bis(trifluoromethylsulphonyl)imide (LiTFSI)-LLZTO (PLL) solid electrolyte membrane. In contrast to routine liquid electrolytes with mobile anions, the PLL solid electrolyte contributes to effective immobilization of anions for realizing uniform ion distribution and dendrite-free Li deposition. On the one hand, the active ceramic filler serves as a rigid part to block dendrites and offers an ultimate protection at extreme temperature (34). On the other hand, the polymer–Li salt substrate acts as a soft part to adapt the changes in the electrode for maintaining a closely contacted interface and sufficient cross-boundary ion transportation. Chemical and mechanical interactions between ceramic particles and the polymer matrix result in reduced PEO crystallinity and pinned $TFSI^-$ anions, enabling relatively fast Li^+ conduction and a wide electrochemical stability window. We further successfully demonstrate the application of this flexible membrane in all–solid-state $LiFePO_4$ (LFP)-Li and $LiNi_{0.5}Co_{0.2}Mn_{0.3}O_2$ (NCM)-Li batteries and manage to obtain dendrite-free LMBs.

Results and Discussion

To link polymer chains onto $TFSI^-$ anions and LLZTO particles intensively, a PEO substrate was mixed with Li salts at first, and then LLZTO particles were added with continual rapid stirring at 65 °C, which was slightly above the melting point of PEO. During the fast mixing at elevated temperature, PEO chains can be fibrillated mechanically and partially entangled with $TFSI^-$ anions and LLZTO particles. When cooled down to room temperature, the polymer chains were pinned locally, leading to the increase of noncrystallized PEO with immobilized anions.

The as-obtained PLL composite electrolyte is freestanding, is mechanically flexible, and can be fully bended (Fig. 2 *A* and *B*), making it feasible for fabricating flexible solid-state batteries. Detailed morphology was characterized by scanning electron microscopy (SEM). The PLL membrane exhibits a clear and smooth surface with few protuberances (Fig. 2*C*). The cross-section image indicates a thickness of around 30 μm, from which it can be clearly observed that the PEO-Li salt polymer and ceramic particles are fully intermingled (Fig. 2*D*).

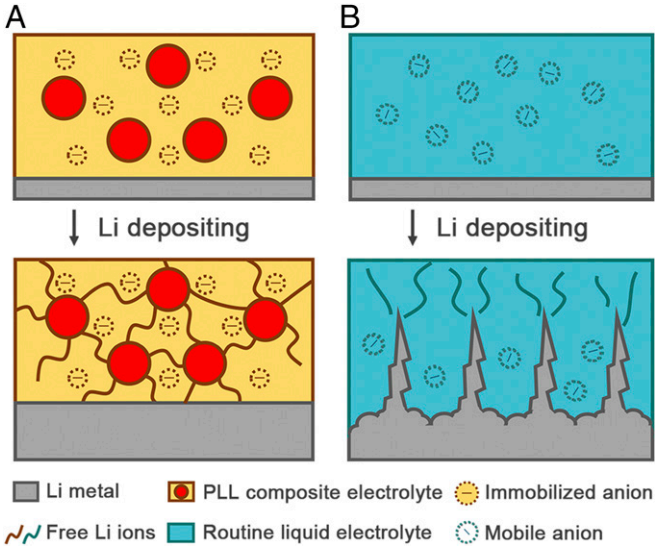

Fig. 1. Schematic of the electrochemical deposition behavior of the Li metal anode with (*A*) the PLL solid electrolyte with immobilized anions and (*B*) the routine liquid electrolyte with mobile anions.

X-ray diffraction (XRD) patterns were conducted to investigate the crystallinity (Fig. 2*E*). LLZTO acts as the most rigid part in the composite membrane. Nearly all diffraction peaks of LLZTO powders match well with the standard pattern of the known garnet phase $Li_5La_3Nb_2O_{12}$ (Powder Diffraction File 80-0457), while signals of other impurities are below the detection limit. $Li_5La_3M_2O_5$ (M = Nb, Ta) is widely accepted as a model with a typical garnet-type cubic structure to identify the crystalline composition of LLZTO (35). This well-matched curve indicates the garnet-type crystalline nature of LLZTO, which is regarded as a promising oxide electrolyte for solid-state LMBs due to its high ionic conductivity, excellent electrochemical stability, and outstanding mechanical properties such as a shear modulus of 55 GPa (36, 37). Another critical part in the electrolyte is the soft PEO matrix. There are strong and sharp characteristic peaks in the XRD pattern of pure PEO membrane, indicating its crystallizing tendency at room temperature. However, the intensities of its characteristic peaks drop markedly upon the addition of Li salts, indicating the reduction of PEO crystallinity. In the PLL composite electrolyte, all components are integrated without losing their own identities. The weakened peaks of PEO also suggest the increase of PEO phase with low crystallinity. The polymer chains in amorphous PEO phase can wrap and immobilize anions, which is crucial for high ionic conductivity of a composite electrolyte.

Thermogravimetric analysis (TGA) was employed to evaluate the thermal stability of various electrolytes (*SI Appendix*, Fig. S1). All three electrolytes, i.e., PEO, LiTFSI-PEO, and PLL, are relatively stable until 300 °C, in sharp contrast to thermally unstable and volatile organic liquid electrolytes (21). As the temperature rises, PEO decomposes at 350–400 °C; while in the TGA curve of LiTFSI-PEO, the slope above 400 °C is ascribed to the decomposition of LiTFSI. The vanishing of polymer significantly threatens the survival of electrolyte membranes. Little weight was retained above 500 °C in both PEO and PEO-LiTFSI electrolytes. The cathode and anode will meet directly, raising serious safety issues at this condition. Nevertheless, as for the PLL composite electrolyte, there is 42.6% of initial weight left at a temperature of 800 °C, which is 10 times higher than that of ceramic-filler–free electrolytes. This indicates the extraordinary thermal stability of remaining LLZTO fillers, which thereby act as a barrier between electrodes at extreme conditions and ensure safety.

The electrochemical stability window is a determinant factor for electrolytes applied in high-voltage Li batteries toward high-energy densities. It can be obtained from the linear sweep voltammetry of the tested electrolyte sandwiched between a Li counter electrode and a stainless steel working electrode. The PLL composite electrolyte (with 40% LLZTO ceramic particles) exhibits a voltage window as large as 5.5 V without distinct reaction (*SI Appendix*, Figs. S2 and S3), indicating its good tolerance to polarization and great potential for high-voltage Li batteries. The key lies in the addition of LLZTO particles, which widens the voltage window from less than 5.0–5.5 V. LLZTO and its surface passivation layer render excellent electrochemical stability against the Li metal, and finely dispersed ceramic fillers help to remove impurities from the interfaces. All of these account for the enhanced stability of PLL composite solid electrolyte in a working battery.

The conductivity of a composite electrolyte, which is mainly featured by either cation or vacancy conduction, is a key factor for practical applications. The PLL composite electrolyte renders low electrical conductivity according to potentiostatic coulometry measurements under various bending states (*SI Appendix*, Fig. S4). The ionic conductivities of PLL composite electrolyte with different LLZTO contents were evaluated by electrochemical impedance spectroscopy (EIS). Symmetric cells were utilized for the

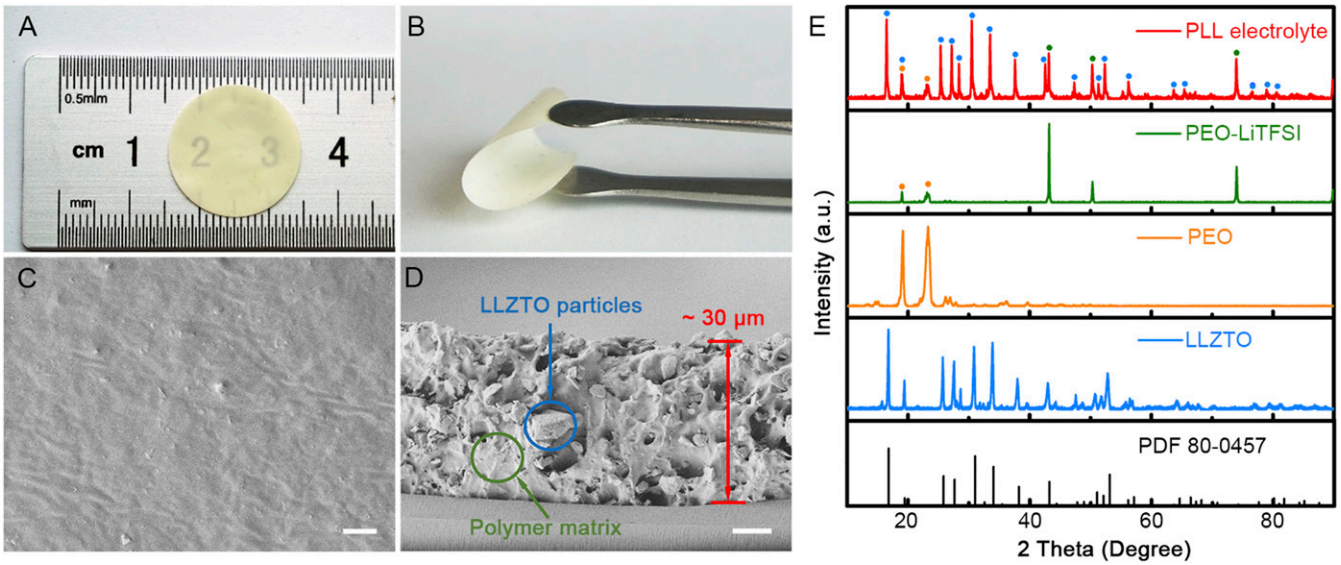

Fig. 2. Morphological and structural characterization for the PLL composite solid electrolyte. (*A* and *B*) Digital images of the PLL electrolyte at (*A*) flat and (*B*) bended states. (*C* and *D*) SEM images of (*C*) the surface and (*D*) a cross-section of the PLL electrolyte. (*E*) XRD patterns of the PLL electrolyte (red), the PEO-LiTFSI electrolyte (green), pure PEO membrane (orange), LLZTO powders (blue), and the powder diffraction file (PDF) of $Li_5La_2Nb_2O_{12}$. (Scale bars in *C* and *D*, 10 μm.)

measurements, consisting of two identical stainless steel foils as blocking electrodes and a PLL electrolyte membrane sandwiched in between (*SI Appendix*, Figs. S5 and S6). The evaluation was conducted at 20–80 °C. An Arrhenius plot of ionic conductivity was obtained correspondingly, along with a well-fitted EIS spectrum at 25 °C (Fig. 3*A*). An intercept of a real axis and an inclined tail appear in each EIS spectrum. The intercept at high frequency was used for calculating the ionic conductivity based on the membrane thickness and the electrode surface area (38). The straight line at low frequency represents the migration of Li ions and reveals the interfacial inhomogeneity. The PLL composite electrolyte with 40% LLZTO content has a preferable ionic conductivity of 1.12×10^{-5} S·cm^{-1} at 25 °C, probably because the multiple ion conducting channels consisting of polymer segments, LLZTO crystals, and heterogeneous interfaces performed and cooperated the best with the moderate ratios. The conductivity increased with the rise of testing temperature. It approaches 10^{-3} S·cm^{-1} at 70 °C, which is comparable to those of liquid electrolytes. Compared with other composite electrolytes with nonactive fillers such as SiO_2 (~2×10^{-6} S·cm^{-1} at room temperature) (39) and Al_2O_3 (1.0×10^{-6} S·cm^{-1} at room temperature) (40), the PLL electrolyte exhibits notable improvements in ionic conductivity at both room and elevated temperatures.

In addition to the relatively high Li ionic conductivity, PLL composite electrolyte with 40% LLZTO also possesses a Li ion transference number (t_+) as high as 0.58 (Fig. 3*B* and *SI Appendix*, Fig. S7 and Table S1). While for the solid composite electrolytes without ceramic fillers (LiTFSI-PEO) and with inadequate ceramic fillers (20% LLZTO) t_+ is 0.37 and 0.38, respectively, indicating that anions are not fixed effectively. The t_+ of routine liquid electrolytes is as limited as 0.22 in 1.0 M $LiPF_6$–ethylene carbonate/diethyl carbonate (EC/DEC = 1:1, in volume) and 0.21 in 1.0 M LiTFSI–1,3-dioxolane/dimethoxyethane (DOL/DME = 1:1, in volume). The low t_+ of routine liquid electrolytes reflects ineffective transportation of Li ions, which leads to a strong space charge near the anode and hence dendritic Li deposition. In contrast, the PLL composite electrolyte with a high t_+ is expected to effectively protect the Li metal anode in a working battery.

The advantage of the high-t_+ PLL composite electrolyte is illustrated by modeling the distribution of Li ions on the anode surface (Fig. 3 *C* and *D*). Uniformly distributed Li ions can guide dendrite-free Li deposition. In the electrolyte with mobile anions (featured by small t_+), free anions tend to move in the opposite direction to cations, becoming a barrier for cation transportation

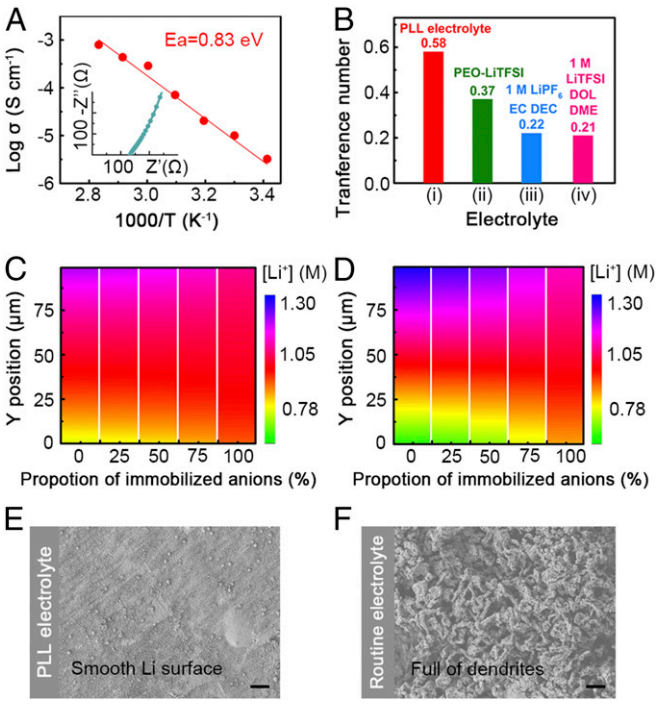

Fig. 3. Diffusion behaviors of Li ions in the PLL electrolyte. (*A*) The Arrhenius plot of the PLL electrolyte at temperatures from 20 °C to 80 °C. *Inset* shows the EIS spectrum of the electrolyte at room temperature (25 °C). (*B*) t_+ of (*i*) PLL composite electrolyte, (*ii*) PEO-LiTFSI solid electrolyte, (*iii*) 1 M $LiPF_6$-EC/DEC, and (*iv*) 1 M LiTFSI-DOL/DME liquid electrolytes. (*C* and *D*) t_+ from the anode surface to the bulk electrolyte (*C*) after 1.0 s and (*D*) at the steady state with 0%, 25%, 50%, 75%, and 100% of immobilized anions. These results were obtained from the finite-element method (FEM). (*E* and *F*) SEM images of Li metal plating on Cu foils with the presence of (*E*) PLL and (*F*) routine liquid electrolytes (1 M $LiPF_6$-EC/DEC). (Scale bars in *E* and *F*, 10 μm.)

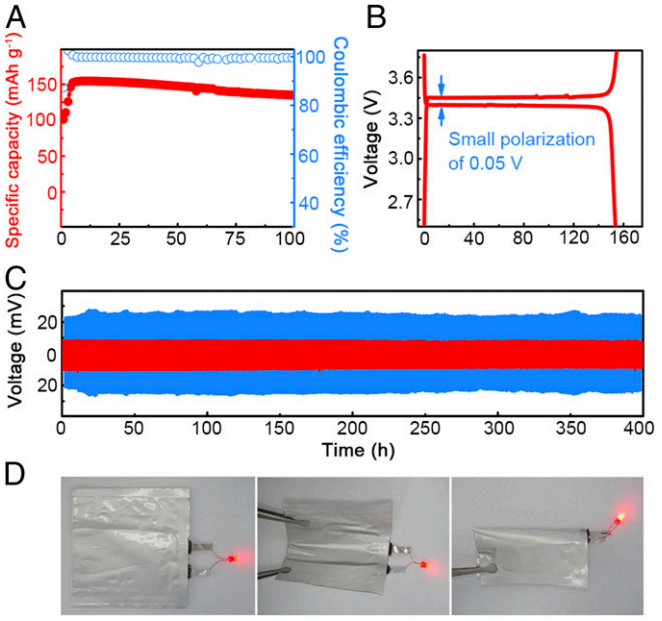

Fig. 4. Electrochemical cycling performance of the PLL electrolyte. (*A* and *B*) Cycling performance (*A*) and corresponding galvanostatic discharge/charge profile (*B*) of the all–solid-state LFP | Li metal battery at a rate of 0.1 C and at 60 °C (1.0 C = 180 mA·g^{-1}). (*C*) Voltage profiles of the lithium plating/stripping in a Li–Li symmetrical cell with PLL (60 °C) and routine liquid electrolytes (25 °C) at a current density of 0.10 mA·cm^{-2}. (*D*) An all–solid-state NCM | PLL electrolyte | Li metal pouch cell was assembled to light the LED at both flat and bended states.

under an applied electric field. Therefore, a large concentration gradient of Li ions forms from the bulk electrolyte to the anode surface. More seriously, such a gradient becomes more predominant with the time of Li deposition extending. When anions are immobilized, it is much easier for Li ions to diffuse from the bulk electrolyte to the anode surface. Hence, a much more harmonious environment is built for uniform Li deposition. Anion immobilization is beneficial for the inhibition of space charge formation, which could induce a homogeneous Li^+ distribution and further lead to a uniform Li deposition. Besides, this surface environment with a uniform distribution of Li ions is established rapidly, exhibiting the potential to reclaim Li ions from disturbance. Therefore, the PLL composite electrolyte with a high t_+, namely a high fraction of immobilized anions, renders uniform distribution of Li ions and hopefully dendrite-free Li deposition.

The influence of the PLL electrolyte (with 40% LLZTO) on the Li deposition was visibly probed by SEM. A total of 0.10 mAh·cm^{-2} of Li metal was deposited on Cu foils at a current density of 0.10 mA·cm^{-2}, with the presence of a PLL solid electrolyte membrane and a 1.0-M $LiPF_6$-EC/DEC liquid electrolyte, respectively (Fig. 3 *E* and *F*). Obviously, Li dendrites grow and accumulate in the liquid electrolyte, forming an extremely uneven surface. Once the dendrites keep growing and reach cathodes, the short circuiting will occur, and this situation is even worse since it is difficult for compliant liquid electrolytes to block dendrites. On the contrary, the PLL composite solid electrolyte contributes to smooth Li deposits and it is also rigid enough for dendrite inhibition (41–44). Compared with Li dendrites deposited in liquid electrolytes, Li metal is plated uniformly and free of dendrites on the Cu foil surface by using the PLL electrolyte.

With excellent mechanical and electrochemical properties proved, the PLL composite electrolyte was applied in all–solid-state lithium batteries. Cells of LFP | Li metal were adopted to demonstrate the cycling performance, which were assembled without liquid electrolyte addition. The all–solid-state batteries exhibited stable cycling capability. A specific capacity of around 155 mAh·g^{-1} and a Coulombic efficiency of 99% were retained (0.1 C) at 60 °C (Fig. 4*A*). The cells maintain excellent cycling performance with 13% capacity fade in 100 cycles, indicating the potential of PLL composite electrolytes in practical applications. Flat plateaus appeared in both charge and discharge profiles, and polarization during cycling was as limited as 0.05 V (Fig. 4*B*). Although batteries with PLL electrolytes are promising for future applications, it is noteworthy that there are limitations resulting from elevated temperature operation, including a more sophisticated battery management system (BMS), limited applications in some consumer electronics, and longer startup time, etc. Much more effort is needed to conquer these issues.

The long-term electrochemical stability of PLL composite solid electrolytes against the Li metal was evaluated by using symmetrical Li | Li cells. The electrolyte membrane was sandwiched between two Li metal foils. The Li metal was plated and stripped time after time to mimic a practical cycling process. Fig. 4*C* and *SI Appendix*, Figs. S8 and S9*A* display voltage profiles of cells cycled at a current density of 0.10 mA·cm^{-2}. The cell with the PLL electrolyte exhibited excellent stability with a nearly constant voltage polarization of 15 mV during the 400-h cycling. Li | Li cells at a current density of 0.20 mA·cm^{-2} also render a stable cycling with a polarization as limited as 60 mV for 800 h (*SI Appendix*, Fig. S10). The interfacial resistances between PLL electrolyte and Li metal before and after cycling are all below 15 Ω (*SI Appendix*, Fig. S11 and Table S2), which are much lower than that of a routine liquid electrolyte (~70 Ω; *SI Appendix*, Table S1). Besides, the resistance was even slightly reduced after 100 cycles, owing to the enhancement of interface optimization after cycles. The interface between PLL electrolyte and Li anode remained stable during cycling, from which a safe battery will benefit a lot. However, the interface was unstable in a routine liquid electrolyte at both room and elevated temperatures (Fig. 4*C* and *SI Appendix*, Figs. S8, S9, and S12). The voltage polarization was severer than that of the cell with the PLL electrolyte, indicating large fluctuations upon cycling. This can be ascribed to the uneven Li plating/stripping and heterogeneous Li metal/electrolyte interface. The remarkable performance of the PLL composite electrolyte against liquid electrolytes results from the fixed anions, homogeneous ion distribution, and fast transport of Li ions.

To demonstrate the versatility of the PLL composite electrolyte, an all–solid-state NCM | PLL electrolyte | Li metal pouch cell was assembled to light a light-emitting diode (LED) (Fig. 4*D*). The LED can be lighted whenever the pouch cell is flat or bended, indicating the ability of the PLL composite electrolyte to be applied in flexible devices. Therefore, the PLL composite electrolyte can not only stabilize the Li metal anode, suppress Li dendrite growth, and enhance the safety of LMBs, but also hold promise for flexible and wearable electronics.

The improved electrochemical performance of Li metal anodes cycled with the PLL solid electrolyte can be attributed to two factors. First, anions as large as $TFSI^-$ can be firmly trapped by PEO chains and LLZTO particles. Fixed anions contribute to

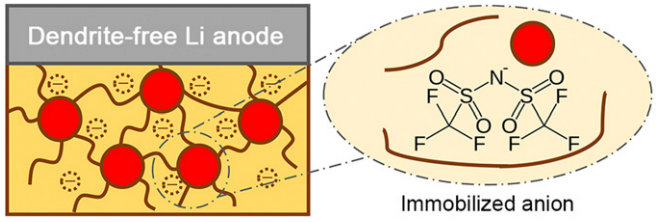

Fig. 5. Schematic of the immobilized anions tethered to polymer chains and LLZTO ceramic particles.

an improved conductivity (24) and dendrite-free Li deposition (45). Second, the relatively slow dynamic response, especially the slow anion movement, helps the PLL solid electrolyte tolerate turbulence during cycling. An efficient Li metal anode demands homogeneous plating/stripping. However, defects and turbulence are difficult to avoid in a working battery. In liquid electrolytes, ions and electrons travel freely in the interspace. Once a tiny Li dendrite forms, the local electrical field will change rapidly, making it easier for subsequent Li deposition on the existing tip. The deposited Li continuously acts as a preferential deposition spot, resulting in endless Li growth. Finally, a hazardous dendrite appears. This domino effect leads to easy loss in efficiency. On the contrary, in the solid electrolyte with immobilized anions, the turbulence in ion distribution can be tolerated due to the slow transport of anions. Ions move uniformly, driven by the electric field, resulting in continuously homogeneous deposition of Li metal (46, 47).

To better understand the origin and role of immobilized anions in the PLL composite electrolyte, diffusion behaviors of Li ions in the electrolyte are thoroughly investigated. Li ions in the composite electrolyte can move through three conducting channels: (*i*) LLZTO particles whose content is above the percolation threshold (48), (*ii*) the PEO-Li salt substrate with reduced polymer crystallinity and enhanced Li salt dissociation, and (*iii*) interfaces between ceramic fillers and the polymer matrix with immobilized anions (Fig. 5).

Li ion channels within the LLZTO crystals are constructed from $(La_3Ta_2O_{12})_n^-$ chains interconnected through Li and La ions. In this work, the LLZTO ceramic used in the PLL electrolyte was sintered with an excess amount of Li precursors. As a result, the number of Li ions (or atoms) is beyond the number of tetrahedral sites, resulting in the occupation of octahedral sites by excess Li and shortening of the Li–Li distance. The electrostatic repulsion between the fairly close Li ions, together with the dynamic process, pushes Li ions to move along the transport channels in the LLZTO crystal (49). Previous ab initio calculations revealed that Li ions migrated in a priority sequence of octahedral site, tetrahedral site, and vacant octahedral site (27). In addition, Li_2CO_3 is widely believed to form on the surface of LLZTO exposed in air, which may also help Li ions migrate, following an interstitial–substitutional exchange (knockoff) mechanism (48, 50).

Chains in the polymer substrate are known to transport Li ions through segmental motions, which will be promoted in amorphous regions (51, 52). Differential scanning calorimetry (DSC) was introduced to evaluate the ability of polymer chains in the matrix to move segmentally. *SI Appendix*, Fig. S13 exhibits the DSC curve and *SI Appendix*, Fig. S13, *Inset* shows the enlarged curve at around −40 °C, representing the glass transition temperature (T_g). The PLL composite electrolyte exhibits the lowest T_g of −57 °C and the melting point (T_m), suggesting that it is easiest for PEO segments in the PLL electrolytes to move at ambient temperature. Therefore, the PLL electrolyte is featured with the fastest ion transport. The pure PEO membrane does not show a glass transition. At around 50 °C, a sharp peak appears, corresponding to a quick and regular melting process at the melting point. That is a common characteristic of a large crystallized polymer. By adding Li salts and LLZTO fillers successively, the peak corresponding to polymer melting shifts to a lower temperature, suggesting the increase of amorphous phase. This can also be proved in the cooling part of DSC curves, as well as in XRD results.

Interfaces between heterostructured materials have been witnessed to transport ions, although the mechanisms are still debated (53, 54). In the light of Lewis acid/base theory, it can be proposed that acidic groups on garnet particles and anions in Li salts will link with each other. $TFSI^-$, as a Lewis base, furnishes the electron pair shared by the acidic group and $TFSI^-$ anion (55). The affinity between oxide fillers and Li–salt anions facilitates the dissociation of LiTFSI, after which anions get immobilized while free Li cations emerge and move rapidly along the extended interface.

It was suggested that the polymer with more amorphous phases contributes to the increase of Li ionic conductivity. In recent years, finite-element simulations revealed that ion transportation occurs near the ceramic–polymer interface (56, 57). In addition, Li NMR was also utilized and indicated that Li ions prefer to migrate through the ceramic phase in the $Li_7La_3Zr_2O_{12}$–PEO composite electrolyte system (58). Although the ion migration path in the composite electrolyte is still controversial, all three ion channels contribute to the fast ion conduction in composite electrolytes. It is also possible that in different conditions (such as different temperatures or charge/discharge stages), the three channels perform synergistic roles.

Conclusions

We proposed a flexible anion-immobilized PLL composite electrolyte membrane to inhibit dendrites in a Li metal anode. Through the addition of LLZTO particles, the crystallization of PEO is sharply reduced and anions are effectively immobilized due to their interactions with ceramic particles and polymer matrix, resulting in well-distributed Li ions and dendrite-free deposition. The PLL composite electrolyte possesses a high Li ionic conductivity of 1.12×10^{-5} S·cm^{-1} at 25 °C and a wide electrochemical window of 5.5 V. The existence of LLZTO fillers affords a barrier to avoid short circuiting. With such excellent mechanical and electrochemical properties, the PLL composite electrolyte was applied in all–solid-state LMBs and achieved stable cycling performance with high specific capacities and dendrite-free Li deposition. The development of an anion-immobilized composite electrolyte reveals a promising opportunity for next-generation safe and flexible LMBs.

Materials and Methods

The PLL composite electrolyte was prepared by first dissolving PEO and LiTFSI. The Al-doped LLZTO powders were added into the solution. The as-obtained slurry was sealed and stirred rapidly at 65 °C until good dispersion. The electrolyte membrane was obtained by doctor blading the slurry on a polytetrafluoroethylene plate. More details on the materials and methods can be found in *SI Appendix*.

ACKNOWLEDGMENTS. The authors thank Kai Liu, Chong Yan, Ying-Zhi Sun, Jin Xie, and Xiao-Ru Chen at Tsinghua University for helpful discussion. This work was supported by the National Key Research and Development Program (Grants 2016YFA0202500, 2016YFA0200102, and 2015CB932500) and the National Natural Science Foundation of China (Grants 21422604 and 21676160).

1. Cheng XB, Zhang R, Zhao CZ, Zhang Q (2017) Toward safe lithium metal anode in rechargeable batteries: A review. *Chem Rev* 117:10403–10473.
2. Zhang R, et al. (2017) Advanced micro/nanostructures for lithium metal anodes. *Adv Sci (Weinh)* 4:1600445.
3. Lin D, Liu Y, Cui Y (2017) Reviving the lithium metal anode for high-energy batteries. *Nat Nanotechnol* 12:194–206.
4. Lu D, et al. (2017) Formation of reversible solid electrolyte interface on graphite surface from concentrated electrolytes. *Nano Lett* 17:1602–1609.
5. Fang R, et al. (2017) More reliable lithium-sulfur batteries: Status, solutions and prospects. *Adv Mater* 29:1606823.
6. Lin D, et al. (2017) Three-dimensional stable lithium metal anode with nanoscale lithium islands embedded in ionically conductive solid matrix. *Proc Natl Acad Sci USA* 114:4613–4618.
7. Zhao C-Z, et al. (2016) Li_2S_5-based ternary-salt electrolyte for robust lithium metal anode. *Energy Storage Mater* 3:77–84.
8. Cheng XB, et al. (2015) A review of solid electrolyte interphases on lithium metal anode. *Adv Sci* 3:1500213.
9. Yan C, et al. (2016) Lithium metal protection through *in-situ* formed solid electrolyte interphase in lithium-sulfur batteries: The role of polysulfides on lithium anode. *J Power Sources* 327:212–220.
10. Cheng X-B, et al. (2017) Implantable solid electrolyte interphase in lithium-metal batteries. *Chem* 2:258–270.
11. Cheng X-B, et al. (2017) Sulfurized solid electrolyte interphases with a rapid Li+ diffusion on dendrite-free Li metal anodes. *Energy Storage Mater*, 10.1016/j.ensm.2017.03.008.
12. Liu B, et al. (2017) Stabilization of Li metal anode in DMSO-based electrolytes via optimization of salt-solvent coordination for Li-O_2 batteries. *Adv Energy Mater* 7:1602605.

13. Manthiram A, Chung S-H, Zu C (2015) Lithium-sulfur batteries: Progress and prospects. *Adv Mater* 27:1980–2006.
14. Zhang X-Q, Cheng X-B, Chen X, Yan C, Zhang Q (2017) Fluoroethylene carbonate additives to render uniform Li deposits in lithium metal batteries. *Adv Funct Mater* 27: 1605989.
15. Li Q, Zhu S, Lu Y (2017) 3D porous Cu current collector/Li-metal composite anode for stable lithium-metal batteries. *Adv Funct Mater* 27:1606422.
16. Lin D, Zhuo D, Liu Y, Cui Y (2016) All-integrated bifunctional separator for Li dendrite detection via novel solution synthesis of a thermostable polyimide separator. *J Am Chem Soc* 138:11044–11050.
17. Liu K, Bai P, Bazant MZ, Wang C-A, Li J (2017) A soft non-porous separator and its effectiveness in stabilizing Li metal anodes cycling at 10 mA cm^{-2} observed in situ in a capillary cell. *J Mater Chem A* 5:4300–4307.
18. Tikekar MD, Choudhury S, Tu Z, Archer LA (2016) Design principles for electrolytes and interfaces for stable lithium-metal batteries. *Nat Energy* 1:16114.
19. Tu Z, et al. (2017) Nanoporous hybrid electrolytes for high-energy batteries based on reactive metal anodes. *Adv Energy Mater* 7:1602367.
20. Zhang R, et al. (2017) Lithiophilic sites in doped graphene guide uniform lithium nucleation for dendrite-free lithium metal anodes. *Angew Chem Int Ed Engl* 56: 7764–7768.
21. Fu KK, et al. (2016) Flexible, solid-state, ion-conducting membrane with 3D garnet nanofiber networks for lithium batteries. *Proc Natl Acad Sci USA* 113:7094–7099.
22. Jayaprakash N, Jones WD, Moganty SS, Archer LA (2012) Composite lithium battery anodes based on carbon@Co_3O_4 nanostructures: Synthesis and characterization. *J Power Sources* 200:53–58.
23. Lu Y, Korf K, Kambe Y, Tu Z, Archer LA (2014) Ionic-liquid-nanoparticle hybrid electrolytes: Applications in lithium metal batteries. *Angew Chem Int Ed Engl* 53:488–492.
24. Tikekar MD, Archer LA, Koch DL (2014) Stability analysis of electrodeposition across a structured electrolyte with immobilized anions. *J Electrochem Soc* 161:A847–A855.
25. Long P, Xu Q, Peng G, Yao X, Xu X (2016) NiS nanorods as cathode materials for all-solid-state lithium batteries with excellent rate capability and cycling stability. *ChemElectroChem* 3:764–769.
26. Chen R, Qu W, Guo X, Li L, Wu F (2016) The pursuit of solid-state electrolytes for lithium batteries: From comprehensive insight to emerging horizons. *Mater Horiz* 3: 487–516.
27. Thangadurai V, Narayanan S, Pinzaru D (2014) Garnet-type solid-state fast Li ion conductors for Li batteries: Critical review. *Chem Soc Rev* 43:4714–4727.
28. Luo W, et al. (2017) Reducing interfacial resistance between garnet-structured solid-state electrolyte and Li-metal anode by a germanium layer. *Adv Mater* 29:1606042.
29. Erickson EM, et al. (2015) Review-development of advanced rechargeable batteries: A continuous challenge in the choice of suitable electrolyte solutions. *J Electrochem Soc* 162:A2424–A2438.
30. Liu W, et al. (2017) Enhancing ionic conductivity in composite polymer electrolytes with well-aligned ceramic nanowires. *Nat Energy* 2:17035.
31. Yue L, et al. (2016) All solid-state polymer electrolytes for high-performance lithium ion batteries. *Energy Storage Mater* 5:139–164.
32. Ren Y, et al. (2015) Oxide electrolytes for lithium batteries. *J Am Ceram Soc* 98: 3603–3623.
33. Li JC, Ma C, Chi MF, Liang CD, Dudney NJ (2015) Solid electrolyte: The key for high-voltage lithium batteries. *Adv Energy Mater* 5:1401408.
34. Liu K, Wang C-A (2014) Garnet-type $Li_{6.4}La_3Zr_{1.4}Ta_{0.6}O_{12}$ thin sheet: Fabrication and application in lithium–hydrogen peroxide semi-fuel cell. *Electrochem Commun* 48: 147–150.
35. Luo W, et al. (2016) Transition from superlithiophobicity to superlithiophilicity of garnet solid-state electrolyte. *J Am Chem Soc* 138:12258–12262.
36. Ni JE, Case ED, Sakamoto JS, Rangasamy E, Wolfenstine JB (2012) Room temperature elastic moduli and Vickers hardness of hot-pressed LLZO cubic garnet. *J Mater Sci* 47: 7978–7985.
37. Yu S, et al. (2016) Elastic properties of the solid electrolyte $Li_7La_3Zr_2O_{12}$ (LLZO). *Chem Mater* 28:197–206.
38. Li Y, et al. (2016) Mastering the interface for advanced all-solid-state lithium rechargeable batteries. *Proc Natl Acad Sci USA* 113:13313–13317.
39. Fan L, Nan C-W, Zhao S (2003) Effect of modified SiO_2 on the properties of PEO-based polymer electrolytes. *Solid State Ion* 164:81–86.
40. Croce F, et al. (2001) Role of the ceramic fillers in enhancing the transport properties of composite polymer electrolytes. *Electrochim Acta* 46:2457–2461.
41. Liu Y, et al. (2017) An artificial solid electrolyte interphase with high Li-ion conductivity, mechanical strength, and flexibility for stable lithium metal anodes. *Adv Mater* 29:1605531.
42. Liu K, et al. (2017) Lithium metal anodes with an adaptive "solid-liquid" interfacial protective layer. *J Am Chem Soc* 139:4815–4820.
43. Yao X, et al. (2016) High-energy all-solid-state lithium batteries with ultralong cycle life. *Nano Lett* 16:7148–7154.
44. Zhang Y, et al. (2017) High-capacity, low-tortuosity, and channel-guided lithium metal anode. *Proc Natl Acad Sci USA* 114:3584–3589.
45. Lu Y, et al. (2015) Stable cycling of lithium metal batteries using high transference number electrolytes. *Adv Energy Mater* 5:1402073.
46. Tu Z, Nath P, Lu Y, Tikekar MD, Archer LA (2015) Nanostructured electrolytes for stable lithium electrodeposition in secondary batteries. *Acc Chem Res* 48:2947–2956.
47. Tikekar MD, Archer LA, Koch DL (2016) Stabilizing electrodeposition in elastic solid electrolytes containing immobilized anions. *Sci Adv* 2:e1600320.
48. Shi S, et al. (2012) Direct calculation of Li-ion transport in the solid electrolyte interphase. *J Am Chem Soc* 134:15476–15487.
49. Yan X, Li Z, Wen Z, Han W (2017) Li/$Li_7La_3Zr_2O_{12}$/$LiFePO_4$ all-solid-state battery with ultrathin nanoscale solid electrolyte. *J Phys Chem C* 121:1431–1435.
50. Shi S, Qi Y, Li H, Hector LG (2013) Defect thermodynamics and diffusion mechanisms in Li_2CO_3 and implications for the solid electrolyte interphase in Li-ion batteries. *J Phys Chem C* 117:8579–8593.
51. Zeng XX, et al. (2016) Reshaping lithium plating/stripping behavior *via* bifunctional polymer electrolyte for room-temperature solid Li metal batteries. *J Am Chem Soc* 138:15825–15828.
52. Zhang JJ, et al. (2015) Safety-reinforced poly(propylene carbonate)-based all-solid-state polymer electrolyte for ambient-temperature solid polymer lithium batteries. *Adv Energy Mater* 5:1501082.
53. Zhou W, et al. (2016) Plating a dendrite-free lithium anode with a polymer/ceramic/polymer sandwich electrolyte. *J Am Chem Soc* 138:9385–9388.
54. Fu KK, et al. (2017) Toward garnet electrolyte-based Li metal batteries: An ultrathin, highly effective, artificial solid-state electrolyte/metallic Li interface. *Sci Adv* 3: e1601659.
55. Lin D, et al. (2016) High ionic conductivity of composite solid polymer electrolyte *via* in situ synthesis of monodispersed SiO_2 nanospheres in poly(ethylene oxide). *Nano Lett* 16:459–465.
56. Kalnaus S, Sabau AS, Tenhaeff WE, Dudney NJ, Daniel C (2012) Design of composite polymer electrolytes for Li ion batteries based on mechanical stability criteria. *J Power Sources* 201:280–287.
57. Kalnaus S, et al. (2013) Analysis of composite electrolytes with sintered reinforcement structure for energy storage applications. *J Power Sources* 241:178–185.
58. Zheng J, Tang M, Hu YY (2016) Lithium ion pathway within $Li_7La_3Zr_2O_{12}$ -polyethylene oxide composite electrolytes. *Angew Chem Int Ed Engl* 55:12538–12542.